

SAFER-Nav: Enhancing Safety for Visual Robot Navigation via Segmentation-Aware Fine-Tuning

Geonyeong Ko^{†1}, Giung Lee^{†2}, and Changjoo Nam^{1,3}

¹Dept. of Electronic Engineering, Sogang University, Seoul, Korea

²Dept. of Computer Science, Rice University, Houston, TX, USA

³Vertical Labs, Co., Ltd., Seoul, Korea

[†]Equal contribution

Abstract: Vision-based navigation models, particularly foundation models, generate viable trajectories from RGB observations alone. However, even state-of-the-art transformer- and diffusion-based policies struggle to generalize in unfamiliar deployment environments containing unseen obstacles or shifted conditions. The resulting trajectories often remain goal-directed but unsafe. Existing efforts improve safety through external trajectory correction or internal geometric priors, yet the resulting policies are not trained to explicitly represent obstacle boundaries or traversable free-space structure. To address this, we propose a navigation model that incorporates these structures directly into the policy via fine-tuning and is designed to be compatible with diverse RGB-based backbones. Across multiple robot platforms, indoor environments, and static and dynamic obstacle scenarios, our method reduces collision frequency relative to ViNT, NoMaD, and their CARE-augmented variants while maintaining goal-reaching performance.

Project page: <https://corl-sub-2026.github.io/>

Keywords: Robot navigation and locomotion; Robot safety, alignment, and safe learning-based systems; Collision avoidance; Multi-modal navigation

1 Introduction

Visual and language foundation models have accelerated progress in vision-based navigation. Goal-conditioned navigation models such as GNM [1], ViNT [2], and NoMaD [3], trained on large heterogeneous datasets, have made zero-shot navigation across diverse environments and robot embodiments increasingly feasible. However, reaching the goal does not imply navigating safely. Recent studies show that even modern transformer- and diffusion-based policies still suffer from frequent collisions in cluttered and unfamiliar environments despite high navigation success rates [4, 5].

Recent efforts have begun to address this problem. CARE [5] improves collision avoidance through an external safety module that estimates monocular depth, builds a local obstacle map, and reactively adjusts the trajectory of a pretrained navigation policy without modifying the policy itself. Flow-Nav [6] instead integrates depth priors and conditional flow matching into the policy. Yet neither makes the policy itself represent obstacle boundaries, free space, or safe passage geometry. External correction leaves the policy unchanged, and geometric depth priors encode proximity rather than traversability.

Representing this structure inside the policy closes both gaps: the policy itself, not a separate module, becomes collision-aware, and the safety signal is semantic rather than purely geometric. To this end, we propose SAFER-Nav (Segmentation-Aware Fine-tuning for Enhancing Safety of Robot Navigation), a segmentation-aware navigation model that injects segmentation-derived representations of obstacle regions and traversable free space directly into the policy through fine-tuning, and is designed to be compatible with diverse RGB-based navigation backbones.

Our contributions include: (i) A segmentation-aware design that makes safety a representation-level property of an RGB navigation policy, injecting obstacle and free-space structure into a frozen pre-

trained backbone through a small set of trainable modules. (ii) A fine-tuning scheme that adds this pathway to a pretrained RGB navigation backbone while preserving the goal-conditioned task formulation, the zero-shot waypoint prediction, and the goal-reaching performance. (iii) Real-world validation across multiple robot platforms with differing camera characteristics, two indoor environments differing in illumination and visual appearance, and static and dynamic obstacle scenarios, showing that internalizing safety as a representation-level feature improves obstacle-aware navigation under unfamiliar deployment conditions.

2 Related Work

Goal-conditioned navigation foundation models such as GNM [1], ViNT [2], and NoMaD [3] generalize across environments and robot embodiments when trained on large heterogeneous datasets. However, real-world evaluations show that strong goal-reaching performance does not imply safe navigation: such models suffer from frequent collisions, confusion in visually repetitive scenes, and degraded robustness under distribution shift [4].

Among the safety-oriented extensions that follow, CARE [5] is a representative plug-in approach that improves collision avoidance without additional range sensors or fine-tuning of the policy. It estimates monocular depth from RGB input [7], builds a local obstacle map, and applies APF-based repulsive forces to the predicted trajectory. Since the correction is applied after trajectory prediction, safety remains external to the policy and depends on the accuracy of depth estimation under lighting and appearance variation. FlowNav [6] instead integrates monocular depth priors and conditional flow matching directly into the policy, but its safety signal also remains primarily geometric. In neither case is the policy trained to represent the semantic distinction between traversable and non-traversable scene structure.

We instead learn safety within the policy itself, using segmentation-aware representations to distinguish traversable from non-traversable regions and predict collision-aware waypoints directly.

3 Problem Definition

We consider *goal-conditioned mobile robot navigation* in zero-shot indoor environments. At each step, the policy receives a short history of RGB observations $o_{t-P:t}$, a goal image o_s , and an aligned history of binary segmentation maps $m_{t-P:t}$ that distinguish *traversable* from *non-traversable* regions. The policy is

$$\pi_\theta : (o_{t-P:t}, o_s, m_{t-P:t}) \mapsto (\hat{d}_t, \hat{a}_t), \quad (1)$$

where \hat{d}_t is the predicted temporal distance to the goal and \hat{a}_t is a short-horizon waypoint sequence for local motion planning, parameterized as

$$\hat{a}_t = \left\{ \hat{w}_t^{(h)} \right\}_{h=1}^H, \quad \hat{w}_t^{(h)} = \left(\Delta x^{(h)}, \Delta y^{(h)}, \sin \theta^{(h)}, \cos \theta^{(h)} \right), \quad (2)$$

where H is the waypoint horizon and each waypoint encodes local position and heading in the local frame of the robot. A trajectory is *safe* if its executed path remains within traversable regions; the task is to reach the goal while maintaining safety throughout execution.

4 Proposed Method: SAFER-Nav

SAFER-Nav incorporates segmentation-aware safety information into a pretrained RGB-based navigation policy. As shown in Fig. 1, it comprises an RGB-goal encoder, a segmentation encoder, a representation-level fusion module, and dual action prediction pathways. The RGB-goal branch follows a pretrained navigation backbone, producing a latent representation from the observation history and goal image. In parallel, a trainable segmentation branch converts aligned binary traversability masks into spatiotemporal tokens, refines them with a lightweight transformer, and injects them into the latent representation through attention-based fusion. The refined representation drives the main waypoint and distance heads, while an auxiliary segmentation-only branch predicts a safety-oriented waypoint sequence. At inference, the two predictions are dynamically blended.

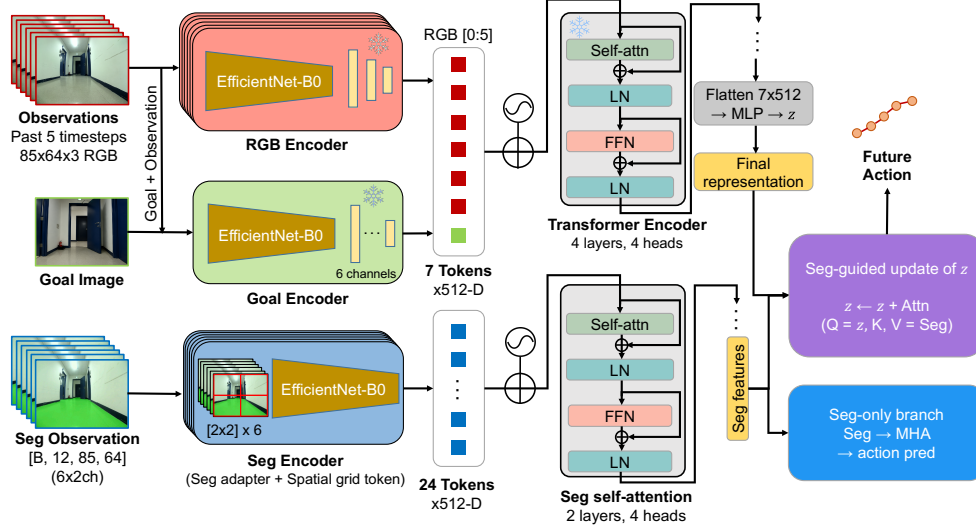


Figure 1: Overview of SAFER-Nav. A trainable segmentation branch augments a pretrained RGB-goal backbone to refine the latent representation and support safety-aware waypoint prediction.

4.1 Input Representation

The model takes three inputs: (i) a sequence of 6 RGB observations $o_{t-P:t}$ with $P = 5$, each $85 \times 64 \times 3$; (ii) a goal image o_s jointly encoded with the current observation following the early-fusion strategy of ViNT; and (iii) aligned binary segmentation masks $m_{t-P:t}$ identifying traversable floor regions. Each mask is a two-channel one-hot tensor, resized via nearest-neighbor interpolation to preserve sharp boundaries, giving a segmentation input of shape $[B, 12, 85, 64]$.

Segmentation labels: Training masks are generated offline from RGB frames using OneFormer [8], a panoptic segmentation model pretrained on ADE20K [9]. Floor-related classes (ADE20K indices 3, 13, and 29) are merged into a single binary mask of traversable regions; the complement forms the non-traversable region. The same model produces masks online at deployment, so no additional human annotation or fine-tuning is required.

4.2 Network Architecture

RGB-goal branch: The RGB-goal branch follows the ViNT architecture. An EfficientNet-B0 [10] observation encoder ψ tokenizes each of the 6 observation frames into a 512-dimensional embedding $\psi(o_i) \in \mathbb{R}^{512}$. A separate EfficientNet-B0 goal-fusion encoder ϕ jointly encodes the current observation and goal image via channel-wise concatenation, producing $\phi(o_t, o_s) \in \mathbb{R}^{512}$. Both encoders are initialized from the pretrained ViNT checkpoint and frozen during training.

Segmentation branch: The segmentation branch consists of an adapter, an encoder, a spatial token grid, and a self-attention block. A 1×1 convolution ($2 \rightarrow 3$ channels) maps the two-channel mask to three channels for EfficientNet-B0 input. A separate EfficientNet-B0, initialized from the observation encoder’s weights, then encodes the adapted mask. Unlike the RGB branch, the segmentation encoder retains the 2×2 spatial structure of the final feature map, yielding 4 tokens per frame, which are projected from 1280 to 512 dimensions for $6 \times 4 = 24$ total tokens. Each token receives two additive positional encodings: a sinusoidal temporal encoding shared across the 4 spatial positions within a frame, and a learnable spatial embedding shared across all 6 frames. The 24 tokens are then refined by a 2-layer pre-norm transformer encoder with GELU activations and a final layer normalization.

Decoder and prediction heads: The 6 observation tokens and the goal token are concatenated and passed to an encoder f with 4 layers and 4 attention heads, increased from ViNT’s 2 to accommodate joint RGB–segmentation reasoning. The output is flattened and projected through an MLP ($3584 \rightarrow 512 \rightarrow 256 \rightarrow 128 \rightarrow 64 \rightarrow 32$) with ReLU activations to produce $\mathbf{z} \in \mathbb{R}^{32}$, which is then refined by the segmentation direct path described below and passed to two prediction heads: a temporal

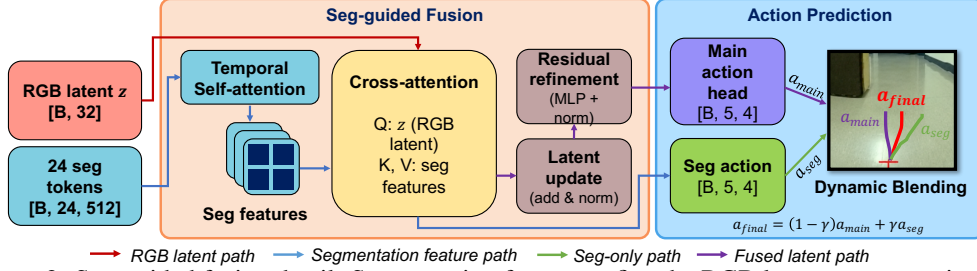


Figure 2: Seg-guided fusion detail. Segmentation features refine the RGB latent representation and support an auxiliary segmentation-only action branch for safety-aware waypoint prediction.

distance $d \in \mathbb{R}$ via a linear layer ($32 \rightarrow 1$), and a sequence of $H = 5$ waypoints $\hat{a} \in \mathbb{R}^{5 \times 4}$ via a 3-layer MLP ($32 \rightarrow 64 \rightarrow 128 \rightarrow 20$) with layer normalization, ReLU, and dropout ($p = 0.1$). Each waypoint is $(\Delta x, \Delta y, \sin \theta, \cos \theta)$ in the local frame of the robot; positions are recovered by cumulative summation, and headings are ℓ_2 -normalized.

4.3 Segmentation-to-Action Mechanisms

As illustrated in Fig. 2, segmentation information influences the policy through two complementary pathways at different stages of the pipeline.

Direct path (after the encoder): After the encoder produces $\mathbf{z} \in \mathbb{R}^{32}$, a residual attention bridge refines it over the segmentation tokens. The representation \mathbf{z} is projected to 512 dimensions and used as a single query attending over the 24 segmentation tokens; the attended vector is projected back to 32 dimensions and added to \mathbf{z} through a residual connection with layer normalization. This update is applied before the main prediction head, enabling late-stage refinement of the action representation given the current obstacle layout.

Segmentation-only action branch (independent): A learnable temporal query $\mathbf{q}_{\text{seg}} \in \mathbb{R}^{512}$ attends over the 24 segmentation tokens to produce a pooled representation. A separate MLP ($512 \rightarrow 256 \rightarrow 128 \rightarrow 20$), with layer normalization, ReLU, and dropout ($p = 0.1$), decodes this into an auxiliary waypoint sequence $\hat{a}_{\text{seg}} \in \mathbb{R}^{5 \times 4}$. This branch is supervised by a *safe target* (defined below) rather than the ground-truth trajectory.

4.4 Training Objective

Our training objective follows the standard supervision used in visual navigation, combining a distance loss and an action loss, augmented with a safety-oriented loss for the segmentation-only branch:

$$\mathcal{L}_{\text{total}} = \lambda_d \mathcal{L}_{\text{dist}} + \lambda_a \mathcal{L}_{\text{action}} + \lambda_s \mathcal{L}_{\text{safe}}. \quad (3)$$

Distance loss $\mathcal{L}_{\text{dist}}$: Mean squared error between the predicted and ground-truth temporal distance to the goal:

$$\mathcal{L}_{\text{dist}} = \frac{1}{B} \sum_{i=1}^B (\hat{d}_i - d_i)^2, \quad (4)$$

where B is the batch size.

Perspective-weighted action loss $\mathcal{L}_{\text{action}}$: MSE between the main action prediction and the ground truth, scaled per sample by the obstacle density with perspective weighting that emphasizes near-field rows. The weight follows $w(y) = \exp(3.0 \cdot y/R)$, where y is the row index and R is the number of image rows, so bottom rows contribute roughly $20\times$ more than top rows when computing the perspective-weighted obstacle ratio $\rho \in [0, 1]$. The per-sample loss weight is $1 + 2\rho \in [1.0, 3.0]$.

Safe target loss $\mathcal{L}_{\text{safe}}$: The segmentation-only branch is supervised by a *safe target* computed online, biasing the trajectory toward free space when obstacles are present. For each sample, the perspective-weighted free-space ratio is estimated on each lateral side of the image, and obstacles are detected by a multi-band analysis over 4 horizontal bands with per-band thresholds, restricted to the central 60% of the image width; far-field bands require obstacle persistence across at least 2

of the 6 frames. Let Δ_{free} denote the left–right free-space difference. A dead zone applies when $|\Delta_{\text{free}}| < 0.05$; otherwise, a lateral avoidance offset is

$$\Delta y_{\text{avoid}} = -\text{sign}(\Delta_{\text{free}}) \cdot \beta \cdot s_{\text{speed}} \cdot c_{\text{free}}, \quad (5)$$

where $\text{sign}(\Delta_{\text{free}})$ indicates the side with more free space, $\beta = 0.5$, $s_{\text{speed}} = \text{clamp}(v_{\text{GT}}/0.5, 0.5, 1.5)$ scales with the ground-truth forward speed, and $c_{\text{free}} = \text{clamp}(|\Delta_{\text{free}}|/0.3, 0.3, 1.0)$ reflects the free-space asymmetry. When an obstacle is detected within the central 30% of the image, a separate confidence term overrides the lateral estimate. The safe target is $\hat{a}_{\text{safe}, y}^{(h)} = \hat{a}_{\text{GT}, y}^{(h)} + \Delta y_{\text{avoid}}$, clamped to $[-0.8, 0.8]$, with the heading recomputed. The safe target loss combines MSE against this target with a hinge-form directional margin,

$$\mathcal{L}_{\text{dir}} = \frac{1}{H} \sum_{h=1}^H \max(0, \mu - \text{sign}(\Delta y_{\text{avoid}}) \cdot \hat{a}_{\text{seg}, y}^{(h)}), \quad (6)$$

weighted by 0.5, where $\mu = 0.05$ is the margin. The term penalizes predictions whose lateral direction opposes the safe avoidance direction, and is active only when avoidance is required.

4.5 Training Details

Training is conducted on the HuRoN dataset [11], which contains 576 indoor trajectories from a fisheye camera and yields approximately 145k training samples after a 6-frame sliding window. Each trajectory is paired with binary traversability masks generated by OneFormer. The network is initialized from the pretrained ViNT checkpoint. The RGB observation encoder, the goal-fusion encoder, and the RGB transformer remain frozen. The segmentation encoder is initialized from the observation encoder’s weights, the segmentation adapter uses Kaiming-uniform initialization, and the remaining new modules are initialized from scratch. All new modules are trained at learning rate 1×10^{-4} for 30 epochs with batch size 64, using AdamW with cosine decay and a 3-epoch linear warmup. The loss weights are $\lambda_d = 0.005$, $\lambda_a = 0.5$, $\lambda_s = 0.3$. Training runs on a single NVIDIA RTX PRO 6000 GPU and takes about 3 hours.

4.6 Inference: Dynamic Action Blending

At deployment, the main action \hat{a} and the segmentation-only avoidance action \hat{a}_{seg} are predicted at each step and blended as $\hat{a}_{\text{final}} = (1 - \gamma) \hat{a} + \gamma \hat{a}_{\text{seg}}$, where the weight γ depends on the current obstacle layout. The instantaneous weight is

$$\gamma_{\text{now}} = \begin{cases} \gamma_{\text{max}}, & \text{if a multi-band obstacle is detected,} \\ \text{clamp}(\eta\rho, 0, \gamma_{\text{max}}), & \text{otherwise,} \end{cases} \quad (7)$$

with $\eta = 2.0$, $\gamma_{\text{max}} = 0.3$, and ρ the perspective-weighted obstacle ratio. Temporal hysteresis $\gamma = \max(\gamma_{\text{now}}, \delta\gamma_{\text{prev}})$ with $\delta = 0.7$ prevents oscillation when obstacles transiently leave the field of view. When no obstacles are detected, $\gamma = 0$ and the output reduces to the main action.

4.7 Deployment

At each timestep, the live RGB frame is processed in parallel by OneFormer, producing a binary traversability mask, and by a context buffer maintaining the 6-frame observation history. The two streams are passed to SAFER-Nav, and the resulting main and auxiliary predictions are blended as described above. The selected waypoint is published to a PD controller that generates linear and angular velocity commands, following ViNT’s deployment protocol.

5 Experiment

5.1 Experimental Setup

We deploy SAFER-Nav on three mobile robots with different visual characteristics (shown in the Appendix): a DJI RoboMaster S1 with a 120° field-of-view (FOV) camera, a TurtleBot4 with an

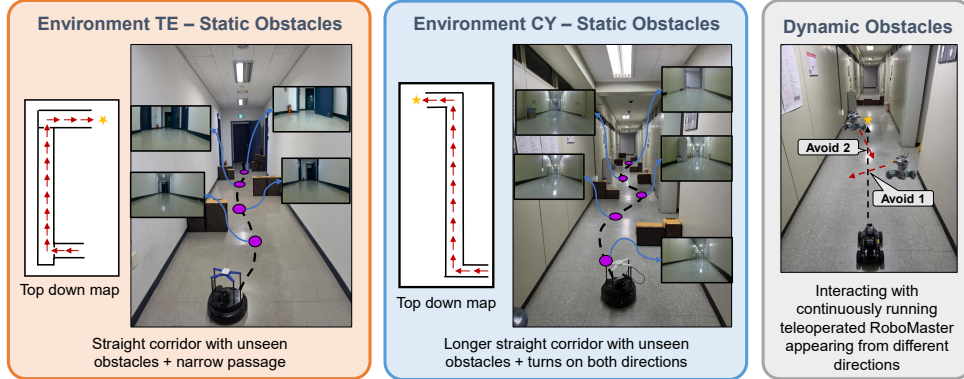


Figure 3: Overview of environments. Left and middle: static-obstacle setups in TE and CY, with maps and representative visual observations. Right: dynamic-obstacle setting, where the robot must continuously avoid the moving robot.

Intel RealSense D435 RGB camera (69.4° FOV), and a LoCoBot with a 170° fisheye camera. All robots operate under the same motion limits for fair comparison: 0.2 m/s linear and 0.8 rad/s angular velocity. The models run on a Lenovo ThinkPad P16 Gen 2 (Intel i7-14700HX, NVIDIA RTX 4090 Laptop, 16 GB).

We compare SAFER-Nav against four baselines (ViNT, NoMaD, ViNT + CARE, NoMaD + CARE) in environments with static and dynamic obstacles (Fig. 3). For static obstacles, we report path length and completion time (lower is more efficient), collision count per run (lower is safer), and arrival rate (higher is better). For dynamic obstacles, we focus on collision rate, as the question is whether the policy maintains safe local behavior under moving interference.

Static environment. We test all methods in two unseen indoor environments, denoted TE and CY, in different buildings and differing in lighting, floor and wall appearance, and geometry. TE is a 15.3 m corridor, 1.78 m wide, with two 90° right turns separated by a straight segment holding eight out-of-distribution (OOD) plastic-box obstacles, ending in a narrow doorway. CY is 24.5 m, 1.7 m wide, with a 90° right turn, a straight segment holding 13 OOD obstacles, and a 90° left turn. Our method is built by fine-tuning ViNT, whose standard deployment constructs a topological graph over the corridor; we follow this setup and place OOD obstacles at random positions along the route at test time. The robot must reach the goal by following the graph while avoiding the inserted obstacles.

Dynamic environment. In CY, we test whether the learned safety behavior extends beyond static clutter by replacing the plastic boxes with a moving mobile robot. Because conventional navigation datasets contain no robot-to-robot encounters, this setup evaluates dynamic obstacle avoidance and OOD generalization simultaneously. The mobile robot continuously crosses the path of the tested robot from arbitrary directions to cover diverse interaction patterns.

5.2 Navigation with Static Obstacles

Table 1 summarizes a comparison of the static-obstacle results across all three robot platforms and both environments. We construct a topological graph over each corridor environment to provide global route information. At test time, we then place multiple OOD obstacles that are not represented in the topological map, forcing the robot to execute consecutive avoidance maneuvers while still reaching the designated goal. For each environment and platform, we run 10 trials.

Across the successful trials, SAFER-Nav achieves the best safety–performance tradeoff on all three platforms, with the highest arrival rate and lowest collision frequency. This consistency shows that the benefit of segmentation-aware adaptation is not tied to a single embodiment or camera view. In TE, SAFER-Nav reaches the goal in 90% of trials with zero collisions on RoboMaster, and maintains similarly strong performance (arrival rate / avg. collision) on TurtleBot4 (90% / 0.24) and LoCoBot (100% / 0.4). The baselines either collide more often or fail to reach the goal reliably. Notably, both ViNT+CARE and NoMaD+CARE underperform their base models on LoCoBot, suggesting that CARE’s external depth-based correction is less well matched to its wider fisheye camera. In

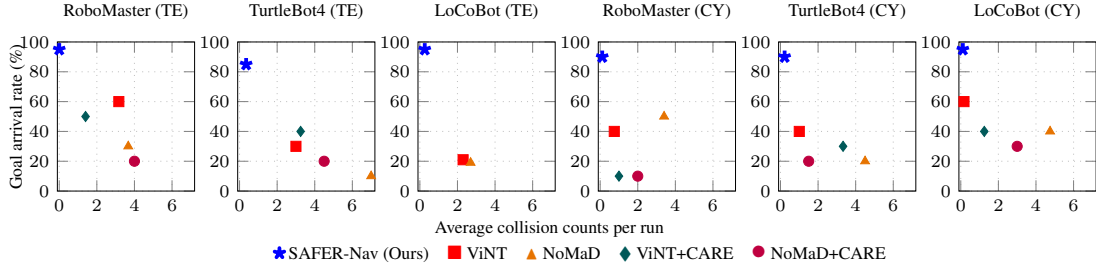


Figure 4: Scatter plot of static-obstacle results: x : average collisions per run; y : goal arrival rate (%). Methods closer to the top-left corner perform better overall, where SAFER-Nav dominates the top-left region across all platforms and environments.

Table 1: Comparison of navigation performance under static obstacle condition. Metrics: goal arrival rate (%), collisions per run, distance (m), and completion time (s).

Robot & Model	Environment TE				Environment CY			
	Goal%	#Coll.	Dist. (m)	Time (s)	Goal%	#Coll.	Dist. (m)	Time (s)
RoboMaster								
SAFER-Nav (Ours)	0.9	0	14.87 ± 0.49	77.91 ± 7.26	0.9	0.22	24.98 ± 0.44	130.84 ± 5.67
ViNT	0.6	3.17	14.59 ± 0.67	79.99 ± 6.95	0.4	0.75	26.20 ± 0.65	128.63 ± 3.12
NoMaD	0.3	3.67	16.38 ± 0.20	87.50 ± 5.72	0.5	3.4	25.48 ± 0.78	122.27 ± 3.70
ViNT + CARE	0.5	1.4	15.17 ± 0.62	82.98 ± 4.22	0.1	1	26.35	138.253
NoMaD + CARE	0.2	4	17.07 ± 1.09	91.75 ± 3.18	0.1	2	25.974	131.193
TurtleBot4								
SAFER-Nav (Ours)	0.9	0.24	14.41 ± 1.09	87.65 ± 7.74	0.9	0.22	25.26 ± 0.74	137.51 ± 3.09
ViNT	0.3	3	15.21 ± 0.52	84.03 ± 2.28	0.4	1	26.12 ± 0.73	141.89 ± 6.90
NoMaD	0.1	7	23.421	120.503	0.2	4.5	26.33 ± 0.15	125.73 ± 5.49
ViNT + CARE	0.4	3.25	14.35 ± 0.28	85.75 ± 4.60	0.3	3.33	26.84 ± 0.28	134.37 ± 3.16
NoMaD + CARE	0.2	4.5	17.28 ± 2.31	107.75 ± 7.07	0.2	1.5	26.08 ± 0.17	147.95 ± 6.16
LoCoBot								
SAFER-Nav (Ours)	1.0	0.4	14.97 ± 0.34	85.13 ± 4.33	1.0	0.1	25.75 ± 0.91	134.63 ± 2.42
ViNT	0.2	2.5	17.18 ± 0.21	82.19 ± 2.74	0.6	0.17	25.88 ± 0.82	126.31 ± 6.09
NoMaD	0.2	2.5	18.78 ± 0.22	102.34 ± 1.23	0.4	4.75	26.14 ± 0.27	129.94 ± 5.83
ViNT + CARE	0	N/A	N/A	N/A	0.4	1.25	25.29 ± 0.14	142.72 ± 4.70
NoMaD + CARE	0	N/A	N/A	N/A	0.3	3	25.92 ± 0.49	152.59 ± 2.18

CY, SAFER-Nav achieves 90% / 0.22 on RoboMaster, 90% / 0.22 on TurtleBot4, and 100% / 0.1 on LoCoBot, while baselines either reach the goal less reliably or make more collisions. Fig. 4 plots goal arrival rate against collision count for all methods, platforms, and environments.

The gains in safety do not come at the cost of efficiency. In TE, the travel distance and completion time of SAFER-Nav stay comparable to ViNT across all platforms, indicating that the reduction in collisions is not achieved through conservative stopping or excessive detours. By contrast, NoMaD inflates both metrics. SAFER-Nav reduces travel distance by up to 39% and completion time by up to 27% relative to NoMaD, because when confronted with unseen obstacles NoMaD repeatedly rotates to search for a feasible subgoal direction and may continue making side-contact collisions before recovering. This is especially costly here, where the robot must avoid multiple OOD obstacles in sequence rather than perform a single correction.

5.3 Navigation with Dynamic Obstacles

We further evaluate SAFER-Nav in CY with a dynamic obstacle (a teleoperated TurtleBot4) to assess whether the learned safety behavior transfers beyond static clutter. Unlike a walking human, whose large image footprint makes them relatively easy to detect, the moving robot presents a substantially smaller and OOD visual target relative to the training data, posing a more demanding test of obstacle awareness. We deploy SAFER-Nav on RoboMaster and evaluate two scenarios: (i) *Corner-appear*, in which the TurtleBot4 enters the field of view from a side corridor, and (ii) *Front-approach*, in which it approaches the RoboMaster head-on and stops in its path.

We run 10 trials per method per scenario (Table 2). ViNT and NoMaD collide in most trials, with near-complete failure in front-approach. CARE-augmented baselines reduce collisions substantially

Table 2: Number of trials with collisions (out of 10) for each dynamic-obstacle scenario.

Model	(i) Corner-appear	(ii) Front-approach
SAFER-Nav (Ours)	0/10	0/10
ViNT	5/10	9/10
NoMaD	6/10	8/10
ViNT + CARE	3/10	2/10
NoMaD + CARE	2/10	2/10

in front-approach, likely because depth-based repulsion detects the approaching robot once it occupies sufficient image area. They still collide in corner-appear, however, where the obstacle enters abruptly from the side and may not be captured early enough to trigger repulsion. SAFER-Nav avoids all collisions, indicating that segmentation-aware traversability representations provide reliable dynamic obstacle awareness even for small, OOD targets.

5.4 Ablation Study

To isolate the contribution of each segmentation-to-action mechanism, we compare the full model (direct path + seg-only branch) against two variants that retain only one mechanism.

With only the seg-only branch, the model consistently fails to avoid obstacles and exhibits frequent head-on collisions regardless of training duration. The segmentation tokens have no residual connection to \mathbf{z} , so the obstacle layout captured by the branch cannot refine the main waypoint prediction, and the auxiliary avoidance signal is too weak on its own to compensate through blending. In TE, this variant succeeds in only 1 of 10 trials.

With only the direct path, the robot begins to deviate from straight-line trajectories in the presence of obstacles, indicating that late-stage attention over the segmentation tokens introduces obstacle awareness into \mathbf{z} . However, the avoidance maneuvers remain inconsistent in magnitude and direction; this variant succeeds in 3 of 10 trials in TE, an improvement over the seg-only branch but still insufficient. Without the safe-target supervision from the seg-only branch, the direct path modulates the representation but has no training signal specifying *where* to steer, producing hesitant or insufficient lateral corrections.

Reliable collision avoidance and consistent goal reaching emerge only when both mechanisms operate together. The direct path injects the current obstacle layout into \mathbf{z} through a residual attention bridge, ensuring obstacle awareness in the main action representation. The seg-only branch, supervised by the safe-target loss, provides a directionally consistent avoidance signal of sufficient magnitude. The two pathways are complementary: the direct path determines *that* avoidance is needed, while the seg-only branch determines *how* to avoid.

6 Conclusion

We proposed a segmentation-aware fine-tuning framework that improves safety in zero-shot visual navigation by embedding obstacle and traversability cues into the policy representation. It achieves safer goal-conditioned navigation across multiple robot platforms in static and dynamic indoor environments, and the ablation shows that late refinement with a segmentation-driven auxiliary branch outperforms early fusion. This points toward safety-aware navigation models that transfer across embodiments and extend to other embodied settings such as robotic Vision-Language Navigation.

7 Limitations

Our approach depends on the quality of the segmentation signal, and errors in training labels or online segmentation outputs can degrade safety-aware action prediction. We also validate the design on only a limited set of backbones; broader testing remains future work. SAFER-Nav is also a learned end-to-end policy adaptation without an explicit collision-avoidance module, so it does not regulate when avoidance should begin, leading to overly conservative deviations or delayed reactions in narrow or cluttered environments. The inference-time blending also introduces hyperparameters such as the sensitivity factor η ; learning these in a principled way is left to future work.

References

- [1] D. Shah, A. Sridhar, A. Bhorkar, N. Hirose, and S. Levine. GNM: A general navigation model to drive any robot. In *Proceedings of IEEE International Conference on Robotics and Automation*, pages 7226–7233, 2023.
- [2] D. Shah, A. Sridhar, N. Dashora, K. Stachowicz, K. Black, N. Hirose, and S. Levine. ViNT: A foundation model for visual navigation. In *Conference on Robot Learning*, pages 711–733, 2023.
- [3] A. Sridhar, D. Shah, C. Glossop, and S. Levine. Nomad: Goal masked diffusion policies for navigation and exploration. In *Proceedings of IEEE International Conference on Robotics and Automation*, pages 63–70, 2024.
- [4] M. Guerrier, K. Soma, J. Pavlasek, and G. Beltrame. Can vision foundation models navigate? zero-shot real-world evaluation and lessons learned. *arXiv preprint arXiv:2603.25937*, 2026.
- [5] J. Kim, J. Sim, W. Kim, K. Sycara, and C. Nam. CARE: Enhancing safety of visual navigation through collision avoidance via repulsive estimation. In *Proceedings of IEEE International Conference on Robotics and Automation*, 2025.
- [6] S. Gode, A. Nayak, D. N. Oliveira, M. Krawez, C. Schmid, and W. Burgard. Flownav: Combining flow matching and depth priors for efficient navigation. In *Proceedings of IEEE/RSJ International Conference on Intelligent Robots and Systems*, pages 17762–17768, 2025.
- [7] L. Piccinelli, C. Sakaridis, Y.-H. Yang, M. Segu, S. Li, W. Abbeloos, and L. Van Gool. Unidepthv2: Universal monocular metric depth estimation made simpler. *IEEE Transactions on Pattern Analysis and Machine Intelligence*, 2025.
- [8] J. Jain, J. Li, M. T. Chiu, A. Hassani, N. Orlov, and H. Shi. Oneformer: One transformer to rule universal image segmentation. In *Proceedings of IEEE/CVF Conference on Computer Vision and Pattern Recognition*, pages 2989–2998, 2023.
- [9] B. Zhou, H. Zhao, X. Puig, S. Fidler, A. Barriuso, and A. Torralba. Scene parsing through ADE20k dataset. In *Proceedings of IEEE Conference on Computer Vision and Pattern Recognition*, pages 633–641, 2017.
- [10] M. Tan and Q. Le. Efficientnet: Rethinking model scaling for convolutional neural networks. In *Proceedings of International Conference on Machine Learning*, pages 6105–6114, 2019.
- [11] N. Hirose, D. Shah, A. Sridhar, and S. Levine. SACSOn: Scalable autonomous control for social navigation. *IEEE Robotics and Automation Letters*, 9(1):49–56, 2023.

Appendix

A Experimental Details

We run experiments on three mobile platforms: RoboMaster S1, TurtleBot4, and LocoBot. Figure 5 shows the actual hardware used in our experiments.

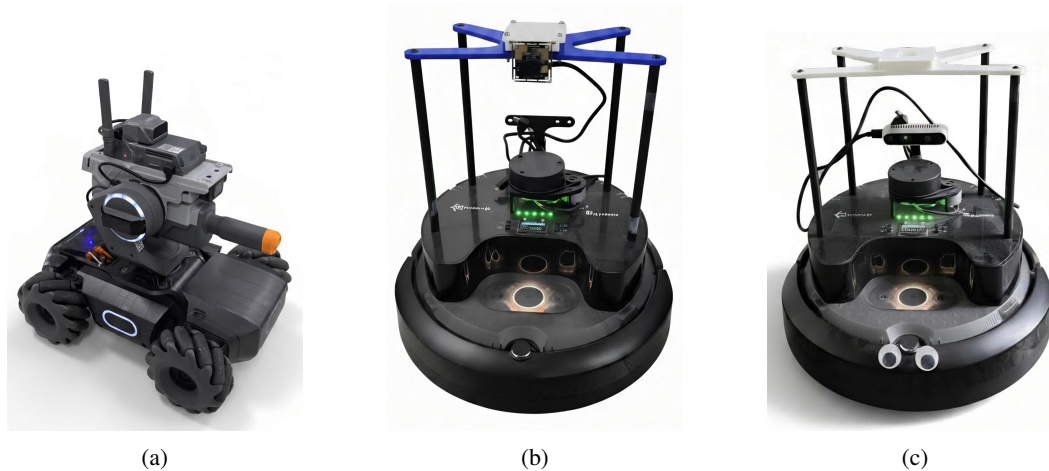


Figure 5: Mobile robot platforms used for evaluation. Each robot was equipped with a monocular RGB camera.

A note for LoCoBot. Although the original LoCoBot is built on a TurtleBot2 base, we implement our LoCoBot using a TurtleBot4 as TurtleBot2 has been discontinued. Nevertheless, two models are both differential drive type with very similar wheelbase width, wheel diameter, and etc. A custom 3D-printed camera mount is designed to match the fisheye camera position.

Table 3: Robot-specific camera and platform parameters.

Specification	LoCoBot	TurtleBot4	RoboMaster S1
Published Image Resolution (pixels)	320×240	320×200	640×360
Robot Size ($L \times W \times H$, mm)	$341 \times 339 \times 350$	$341 \times 339 \times 351$	$320 \times 240 \times 270$
Camera Height (mm)	340	245	240
Camera X-offset (mm)	10	-60	70

- **Published Image Resolution:** The resolution of the RGB images published by each camera over ROS 2.
- **Robot size ($L \times W \times H$):** Physical dimensions of each robot, measured in millimeters (mm).
- **Camera Height:** The vertical distance from the ground to the optical center of the camera.
- **Camera X-offset:** The horizontal distance (in mm) between the geometric center of robots and the camera.
- A positive value indicates a forward-facing offset (camera mounted ahead of center), while a negative value indicates a rear-facing offset.